Open-Source pyMAPOD Framework

Theory Manual

v.beta

Developed by Computational Design Laboratory (CODE Lab)

Department of Aerospace Engineering
Iowa State University
Ames, Iowa

Leading Developers: Leifur Thor Leifsson
Xiaosong Du
Jethro Nagawkar

We gratefully acknowledge the support of the Center for Nondestructive Evaluation Industry/University Cooperative Research Program at Iowa State University

Code and updates are available at the link: https://github.com/CODE-Lab-IASTATE/MAPOD

CONTENTS

1 INTRODUCTION

The process of inspecting, testing, or evaluating materials, components or assemblies for discontinuities, damage (e.g., fatigue cracks) or differences in characteristics without destroying the serviceability of the part or system is called Nondestructive testing (NDT) [1–5]. Modern NDT systems are used in manufacturing, fabrication, and in-service inspections to ensure product integrity and reliability, to control manufacturing processes, lower production costs, and to maintain a uniform quality level. Various NDT detection modalities have been developed, such as ultrasonic testing (UT) [6–10] and electromagnetic testing (ET) [11–14]. UT systems rely on the phenomena of scattering and reflection of ultrasound for inspecting the material under test, and have been successfully and widely introduced to several engineering areas, such as defect inspection on welds [15–18], damage estimation on aircraft [19–22] and flaw characterization under various operation situations [23–26].

Probability of detection (POD) [27–30] is a metric used for quantifying inspection capability of NDT systems. The POD calculation was initially developed and obtained only through experiments. MIL-HDBK-1823A [31] is the key reference for the POD calculation, and MH1823 [32] is a freely available software for calculating POD based on a given set of data.

Sensitivity analysis (SA) [33–37] is an important approach for quantifying the effects of each variability parameter has on the model response of interest. SA can be categorized into two types: (1) local sensitivity analysis [38–41] focused on how a small perturbation near an input space value affects the model response, and (2) global sensitivity analysis [42–47] focused on the variance of model response and more precisely on how the input variability affects the output variance. The global sensitivity analysis method, based on Sobol' indices [48–50] is the most commonly used method for NDT systems, and is also the method we utilized in this work.

Model-assisted probability of detection (MAPOD) [51, 52] is an important terminology used in the field of nondestructive testing (NDT) [53]. It is used to quantify the reliability of the detecting system and can greatly reduce the required experimental information. MAPOD calculations have been widely applied to varieties of NDT areas, such as ultrasonic testing, eddy current testing and x-ray based testing. Researchers, such as J. Aldrin [54, 55], J. Knopp [56], and R. Miorreli [57], have made great progress and improvements in these fields. However, as far as the authors know, most of the MAPOD calculations performed rely on commercial software, such as CIVA. Due to these reasons, the authors decide to develop this open-source MAPOD framework, aiming at providing convenient tools to NDT researchers. The general model-assisted approach for generating the POD curves and SA is shown in Fig. 1

This open-source MAPOD framework is developed in python, which makes it cross-platform. All the necessary python modules require to run the MAPOD framework can be found in the User Manual. An overview of the MAPOD as well as sensitivity analysis can be found in Section 2. Section 2.2 gives details of the necessary steps involved in the metamodeling process. Section 2.4 discusses the SA in detail while 2.3 discusses the POD in detail. Finally, Section 3 presents the spherically-void-defect test

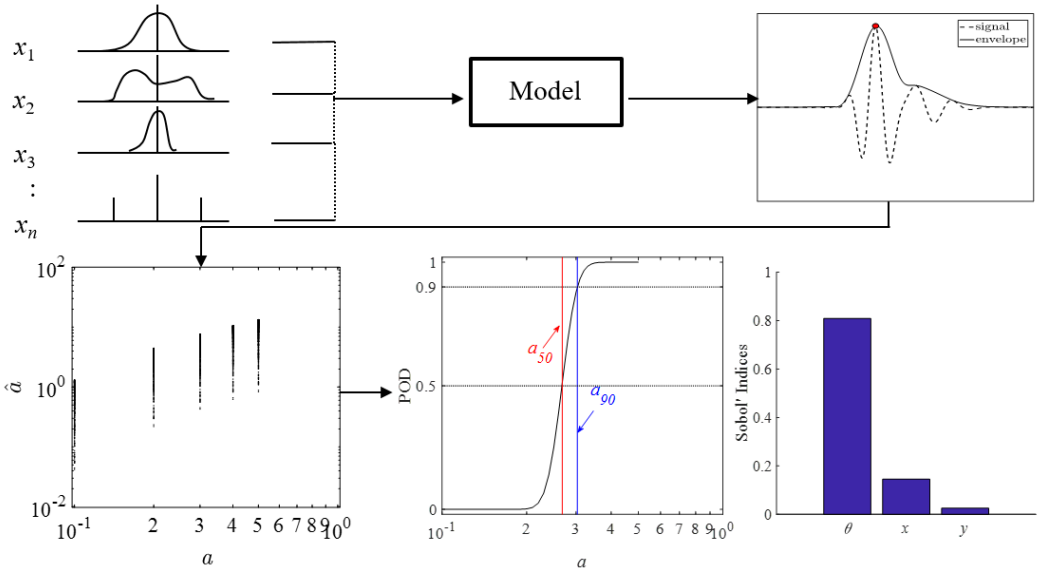

Figure 1: Flowchart showing the model-assisted approach for the calculation of POD and sensitivity analysis.

case and compares the results from the MAPOD framework to those from the MH1823 [32] software.

The Computational Design (CODE) lab would like to thank the Center of Nondestructive Evaluation (CNDE) for funding this program. In addition, we also want to say thanks to our colleagues, Dr. Jiming Song, Dr. William Meeker, Dr. Ronald Roberts and Dr. Leonard Bond for providing us with the physics-based NDT simulation models. We would also like to thank them for their valuable ideas, insights and suggestions.

2 Overview of the pyMAPOD Framework

This section gives a general overview of the pyMAPOD framework, while the subsequent subsections give the detailed description of each process involved in generating the POD curves as well as performing SA. The process starts by sampling the input variables from selected distributions. For these combinations of input variables, either physics-based model simulations or experiments are performed, to obtain the model responses. The "$\hat{a}$ vs. a" regression can then be performed from this data (More on this in Section 2.3.2) or if the data isn't sufficient, a response surface can first be generated, from which model responses can be predicted. Following this step, the POD curve can be generated and/or the SA can be performed. This process is summarized in Fig. 2. Section 2.1 gives the description of the various distributions used in sampling the input data. Section 2.2 introduces the metamodeling process along a detailed description of each metamodel used in this framework. Details of the SA can be found in Section 2.4 while POD analysis can be found in Section 2.3

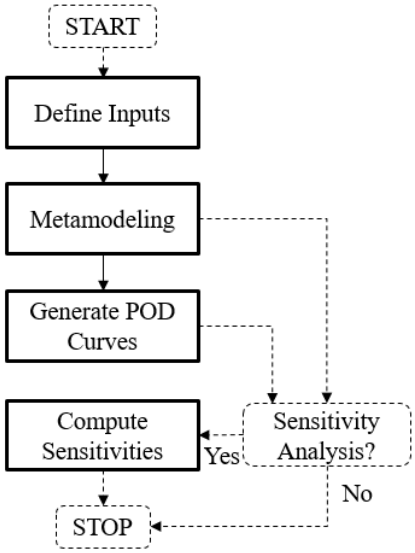

Figure 2: Meta-MAPOD process for POD and sensitivity analysis.

2.1 Defining the Input Distributions

In NDT, the input parameters typically involved are the defect size 'a' along with other uncertainty parameters such as probe angle and location of the transducer from the defect. To generate the POD curves and/or perform SA, these input parameters need to be sampled. The sampling in the framework is done assuming these input parameters to be either of uniform or Gaussian distribution. This section gives an overview of these distributions.

2.1.1 Uniform Distribution

The uniform distribution is represented by

$$X \sim U(a,b), \tag{1}$$

where a is the upper upper limit and b is the lower limit of the intervals. Its probability density function is given by

$$f(x|a,b) = \frac{1}{b-a} \qquad \forall a \leq x \leq b. \tag{2}$$

Figure 3 shows the probability density functions of variables with three different uniform distributions. A uniform distribution implies that all the values of a variable between the interval are equal. Higher the difference between the bounds, lower the probability of each variable. This can be seen in Fig 3, the blue and black lines have lower probabilities compared to the red line, but have higher bounds lengths.

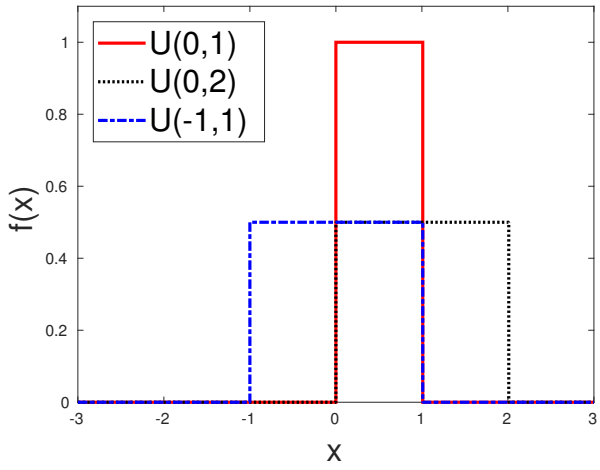

Figure 3: Uniform distribution.

2.1.2 Gaussian Distribution

The Gaussian or normal distribution is represented by

$$X \sim N(\mu, \sigma^2), \tag{3}$$

where μ is the mean of the distribution and σ^2 is the variance. Its probability density function is given by

$$f(x|\mu,\sigma^2) = \frac{1}{\sqrt{2\pi\sigma^2}} \exp^{-\frac{1}{2\sigma^2}(x-\mu)^2} \qquad \forall \infty \leq x \leq \infty. \tag{4}$$

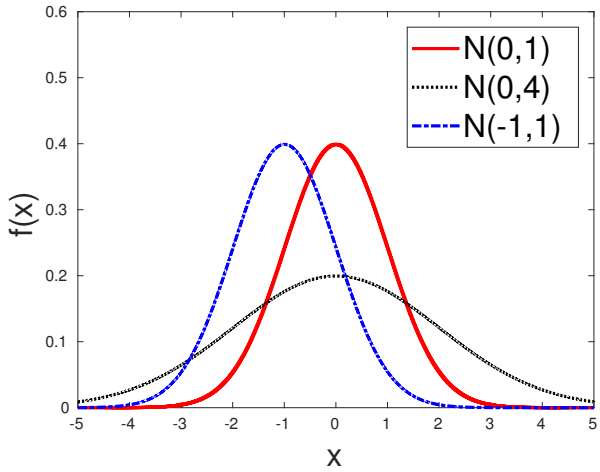

Figure 4: Gaussian distribution.

Figure 4 shows three normal distributions with difference means and variances. In a normal distribution, the highest probability is located at the mean. Changing the mean changes the location of this maximum probability. The variance affects the thickness of the distribution, higher variances have lower peak probabilities, however, probabilities of the variables away from the mean are higher. The red and blue lines in Fig. 4 have the same variance, but different means, affecting the location of the peak probability. The red and black lines have same mean, but different variance, which affects the thickness of the distribution as well as the peak probability value. However, the location of peak probability doesn't change.

2.2 Metamodeling

This section discusses the metamodeling process used for POD analysis (Fig. 5). It gives an overview of the metamodeling process along with the sampling, the metamodel construction process and its validation.

2.2.1 Workflow

The metamodel-based MAPOD process is shown in Fig. 5. It is constructed using the Latin Hypercube sampling (LHS) [58] for the training data set. The training data set is usually generated from physics-based simulation models or experimental data. Various metamodels can then be constructed from this data set. These metamodels are then validated using testing data generated by Monte Carlo sampling (MCS) [59]. The root mean squared error (RMSE) with user-defined accuracy threshold (1% of standard deviation of testing observations) is used to test the accuracy of the metamodels. Resampling is done

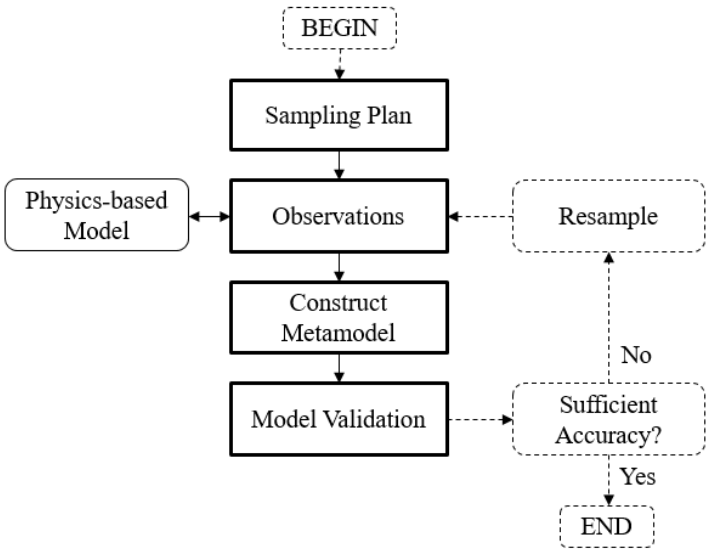

Figure 5: Metamodel-based MAPOD process.

in order to increase the accuracy of the metamodel if necessary. The metamodel-based MAPOD analysis can then be performed.

2.2.2 Sampling

Sampling is the iterative process of drawing values from probability density functions (PDF) associated with the variability parameters. The assigned PDFs are expected to be reconstructed by sufficient sampling. In this framework, the MCS [60] and LHS [61] are used.

The testing points are generated using the MCS method [60]. The sample points are randomly generated using the MCS from anywhere within the variability space. It consists of two main steps: (1) random numbers are generated using the Uniform (0, 1) distribution with replacement, and (2) the random numbers are then used as the probability values of an associated cumulative density functions of the variability parameters. The corresponding parameter values can then be obtained via quantile functions.

To generate the training points, the LHS method [61] is used. The steps used in LHS are similar to those of MCS. However, the first step involves stratifying the PDFs of the variability parameters into equal intervals on the cumulative scale [0, 1]. The random numbers are then generated within this stratified intervals, which prevents "clustered" sample numbers. These numbers are then used as probability values and the parameter values can be obtained via quantile functions.

2.2.3 Construct metamodel

Metamodeling approaches are used to represent physics information in lieu of high-fidelity physics-based simulation models. This section describes the details of the PCE, Kriging and the PC-Kriging metamodels.

2.2.3.1 Polynomial Chaos Expansions

The polynomial chaos expansions (PCE) [62] method has the generalized format

$$Y = M(\mathbf{X}) = \sum_{i=1}^{\infty} \alpha_i \Psi_i(\mathbf{X}), \tag{5}$$

where $\mathbf{X} \in \mathbb{R}^n$ is a vector with random independent components, described by a probability density function f_X. $Y \equiv M(\mathbf{X})$ is a map of $\mathbf{X}$, i is the index of i^{th} polynomial term, $\mathbf{\Psi}$ is multivariate polynomial basis, and α is corresponding coefficient of basis function. In practice, the total number of sample points needed does not have to be infinite, instead, a truncated form of the PCE is used

$$M(\mathbf{X}) \approx M^{PC}(\mathbf{X}) = \sum_{i=1}^{P} \alpha_i \Psi_i(\mathbf{X}), \tag{6}$$

where, $M^{PC}(\mathbf{X})$ is the approximate truncated PCE model, P is the total number of sample points needed, which can be calculated as

$$P = \frac{(p+n)!}{p!n!}, \tag{7}$$

where, p is the required order of PCE, and n is the total number of random variables.

Since a polynomial basis has the characteristics of orthonormality, the equation can be solved by taking the expectation of Eqn. 5 multiplied by Ψ_j,

$$\alpha_i = E[\Psi_i(\mathbf{X}).M(\mathbf{X})], \tag{8}$$

which is called quadrature method [63]. This method works well for low-dimensional problems, but suffers from the "curse of dimensionality".

Another method is to treat the model response as a summation of PCE prediction and corresponding residual

$$M(\mathbf{X}) = M^{PC}(\mathbf{X}) + \epsilon_P = \sum_{i=1}^{P} \alpha_i \Psi_i(\mathbf{X}) + \epsilon_P \equiv \boldsymbol{\alpha}^T \boldsymbol{\Psi}(\mathbf{X}) + \epsilon_P, \tag{9}$$

where, ϵ_P is the residual between $M(\mathbf{X})$ and $M^{PC}(\mathbf{X})$, which is to be minimized using the least-squares methods.

Then the initial problem can be converted to a least-squares minimization problem

$$\hat{\boldsymbol{\alpha}} = \arg\min_{\boldsymbol{\alpha}} E[\boldsymbol{\alpha}^T \boldsymbol{\Psi}(\mathbf{X}) - M(\mathbf{X})]. \tag{10}$$

The first method, used for solving this problem above and applied in this work, is called ordinary least-squares (OLS) [64], with the coefficients obtained by solving

$$\hat{\boldsymbol{\alpha}} = (\mathbf{A}^T\mathbf{A})^{-1}\mathbf{A}^T\mathbf{Y}, \tag{11}$$

where $\mathbf{Y}$ is the vector of model responses at training points, $A_{ji} = \Psi_i(x^j), j = 1,...,n, i = 1,...,P$.

The second method used for solving Eqn. 45, is the least-angle regression sparse (LARS) [65, 66], adding one more regularization term to favor low-rank solution [67]

$$\hat{\boldsymbol{\alpha}} = \arg\min_{\boldsymbol{\alpha}} E[\boldsymbol{\alpha}^T \boldsymbol{\Psi}(\mathbf{X}) - M(\mathbf{X})] + \lambda||\boldsymbol{\alpha}||_1, \tag{12}$$

where λ is a penalty factor, and $||\boldsymbol{\alpha}||_1$ is the L_1norm of the coefficients of the PCE.

The LARS [68] algorithm is based on the sparsity-of-effects principle, meaning that only low-order relationship among inputs are important. These two types of methods used for solving the least-squares minimization problem are very efficient in calculation, and can accept an arbitrary number of sample points.

The mean value of PCE is

$$\mu^{PC} = E[M^{PC}(\mathbf{X})] = \alpha_1, \tag{13}$$

where α_1 is the coefficient of the constant basis term $\Psi_1 = 1$. The standard deviation of PCE is

$$\sigma^{PC} = E[(M^{PC}(\mathbf{X}) - \mu^{PC})^2] = \sum_{i=1}^{P} \alpha_i^2, \tag{14}$$

which is the summation on coefficients of non-constant basis terms only.

2.2.3.2 Kriging

Kriging [69–71] is an interpolation method with the generalized formula written as

$$M^{KR}(\mathbf{X}) = \mathbf{g}^T(\mathbf{X})\boldsymbol{\gamma} + \sigma^2 Z(\mathbf{X}), \tag{15}$$

where $\mathbf{X} \in \mathbb{R}^n$. It consists of two parts, the global trend function, given by $\mathbf{g}^T(\mathbf{X})\boldsymbol{\beta}$ and the local deviation function, given by $\sigma^2\ Z(\mathbf{X})$. $\mathbf{g}^T(\mathbf{X}) = [g_0(\mathbf{X}), ..., g_{p-1}(\mathbf{X})]^T \in \mathbb{R}^p$ is defined as a set of the regression basis functions. $\boldsymbol{\gamma} = [\gamma_0(\mathbf{X}), ..., \gamma_{p-1}(\mathbf{X})]^T \in \mathbb{R}^p$ denotes the vector of the corresponding coefficients. $Z(\mathbf{X})$ is a stationary Gaussian process with zero mean and unit variance, while σ^2 is the constant variance of the Gaussian process. In this framework, a Gaussian exponential spatial correlation function is used, which is written as [72]

$$R(\mathbf{X}, \mathbf{X}') = \exp\left[-\sum_{k=1}^{n}\left(\frac{X_k - X_k'}{h_k}\right)^2\right], \tag{16}$$

where $\mathbf{h} = [h_1, h_2, ..., h_n]^T$ denotes the vector of unknown hyperparameters to be tuned. The Matern-5/2 covariance function is also used and is written as [73]

$$R(\mathbf{X}, \mathbf{X}') = \left[1 + \sqrt{5}\sqrt{\sum_{k=1}^{n}\left(\frac{X_k - X_k'}{h_k}\right)^2} + \frac{5}{3}\sum_{k=1}^{n}\left(\frac{X_k - X_k'}{h_k}\right)^2\right] \exp\left(-\sqrt{5}\sqrt{\sum_{k=1}^{n}\left(\frac{X_k - X_k'}{h_k}\right)^2}\right). \tag{17}$$

To make a prediction $M^{KR}(\mathbf{X})$ from the Kriging response surface, the formula is given by [69]

$$M^{KR}(\mathbf{X}) = \mathbf{g}^T\boldsymbol{\gamma} + \mathbf{r}^T\mathbf{R}^{-1}(\mathbf{Y}_{\text{tr}} - \mathbf{G}\boldsymbol{\gamma}), \tag{18}$$

with a linear trend function $\mathbf{g}^T = [1, X_1, X_2, ..., X_n]$ used in this work. $\mathbf{Y}_{\text{tr}}$ is the vector of training point observations. $G_{ij} = g_j(X_i)$, where $i = 1, 2, ..., N$, $j = 1, 2, ..., N+1$. N is the total number of training points. $\mathbf{r}$ is the cross-correlation vector between each training point and the point to be predicted ($\mathbf{X}$). Here $r_i = R(\mathbf{X}, \mathbf{X}_{tr,i}; \boldsymbol{\gamma})$, where $\mathbf{R}$ is the correlation matrix among the training points with $R_{ik} = R(\mathbf{X}_{tr,i}, \mathbf{X}_{tr,k}; \boldsymbol{\gamma})$, where $i, k = 1, 2, ..., N$, and $\boldsymbol{\gamma}$ and σ^2 are given by

$$\boldsymbol{\gamma} = (\mathbf{G}^T\mathbf{R}^{-1}\mathbf{G})^{-1}\mathbf{G}^T\mathbf{R}^{-1}\mathbf{Y}_{\text{tr}}, \tag{19}$$

and

$$\sigma^2 = 1/N(\mathbf{Y} - \mathbf{G}\boldsymbol{\gamma})^T\mathbf{R}^{-1}(\mathbf{Y}_{\text{tr}} - \mathbf{G}\boldsymbol{\gamma}). \tag{20}$$

The maximum likelihood estimation value of $\mathbf{h}$ is found by solving

$$\hat{\mathbf{h}} = \arg\min_{\mathbf{h}} \left(\frac{1}{2}\log(\det(\mathbf{R})) + \frac{N}{2}\log(2\pi\sigma^2) + N/2 \right). \tag{21}$$

2.2.3.3 Polynomial Chaos-Based Kriging

The Kriging and PCE metamodeling methods can be combined to create a PC-Kriging [74, 75] metamodel. This metamodel combines the advantages of both the PCE and the Kriging metamodels, making it a more effective metamodel. The interpolation-based Kriging metamodel is known to capture the local variations well, while the regression-based PCE is known to capture the global behaviour of the computational model well.

The generalized PC-Kriging metamodel is given by [74]

$$M(\mathbf{X}) \approx M^{PCK}(\mathbf{X}) = \boldsymbol{\alpha}^T \boldsymbol{\Psi}(\mathbf{X}) + \sigma^2 Z(\mathbf{X}), \tag{22}$$

with M^{PCK} being the approximation using the PC-Kriging metamodel. The PC-Kriging metamodel is constructed with the universal Kriging model, with the orthogonal polynomial bases of a PCE metamodel as the trend function. This is given by the first term of right-hand side. The second term is the same as used in Eqn 15, which denotes the constant standard deviation, σ and the zero mean and unit variance stationary Gaussian process, $Z(\mathbf{X})$.

Three main steps are used to construct the PC-Kriging metamodel:

1. The LARS-based PCE is constructed as described in Section 2.2.3.1.
2. The important terms selected by LARS is used as the trend function terms of a universal Kriging model which is used in the construction of the PC-Kriging model.
3. The maximum likelihood estimate (Section 2.2.3.2 is used to calculate the unknown coefficients of the PC-Kriging model in Step 2.

2.2.4 Validation

The RMSE is used to validate the the metamodel and is given by,

$$\text{RMSE} = \sqrt{\sum_{i=1}^{n_t} (\hat{Y}_i - Y_i)^2 / n_t}, \tag{23}$$

with n_t being the total number of testing data, $\hat{Y}_i$ and Y_i being the metamodel estimation and high-fidelity observation respectively at the ith testing point. Given that the model responses are small at small defect sizes, the normalize RMSE (NRMSE) is also calculated at each defect size for further insights. NRMSE is the RMSE divided by a reference quantity of interest. For this framework, the range of high-fidelity model responses at the corresponding defect size is used and has the following expression

$$\text{NRMSE} = \text{RMSE}/(\max(\mathbf{Y}) - \min(\mathbf{Y})). \tag{24}$$

In this framework, the RMSE values of metamodels are required to be equal to or lower than $1\%\sigma_{\text{testing}}$ to have acceptable global accuracy, and the NRMSE values are expected to be within 1% for all defect sizes.

2.3 POD Analysis

This section discusses the POD calculation. Section 2.3.1 introduces the least squares method and the maximum likelihood method used for linear regression. In Section 2.3.2, linear regression is be applied to the "$\hat{a}$ vs. a" regression, followed by POD calculation. Section 2.3.4 gives the details on the calculation of the confidence interval.

2.3.1 Linear regression

2.3.1.1 Introduction

inear regression [76] is a statistical method that allows us to summarize and study relationships between two continuous or quantitative variables: one variable, denoted x, is the independent variable or predictor, while the other one, denoted y, is the dependent variable or response. The linear relationship between x and y is usually given as:

$$y = \beta_0 + \beta_1 \cdot x + \epsilon, \tag{25}$$

where β_0 is the intercept of the regression line, β_1 is the slope of the regression line and ϵ is a Normally distributed random error with a zero-mean and constant standard deviation:

$$\epsilon \sim Normal(0, \sigma_\epsilon^2). \tag{26}$$

This random error accounts for the noise present in the data and is responsible for varying responses y at a fixed x values. This noise may arise from the operating system or from other sources. The predicted value y represents the expected value of the response at the x location (Fig. 6).

As shown above, the only unknowns in linear regression problems are the constants β_0, β_1, and σ_ϵ, which can be solved using various methods. Among all these methods, the least squares (LS) method and the maximum likelihood (ML) method are the most commonly used. Both these methods along with their relationships will be discussed in the following sections.

2.3.1.2 Least squares method

As shown in Eqn. 25, the linear relation is constructed using β_0, β_1, and σ_ϵ. It can be converted as:

$$\epsilon = y - (\beta_0 + \beta_1 \cdot x), \tag{27}$$

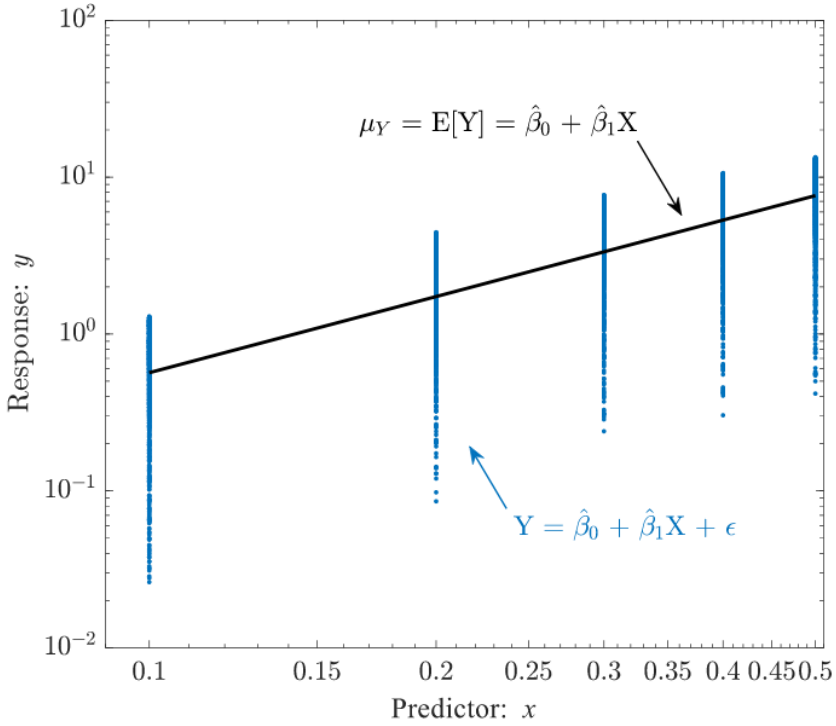

Figure 6: Linear regression line on random observations.

which is the residual between observed values and the estimation from linear regression line. A widely used method for estimating the coefficients is the least squares method [77], which minimizes the sum of the squared of residual at each observed value:

$$min(S) = min \sum_{i=1}^{n} (\epsilon_i)^2 = min \sum_{i=1}^{n} (y - (\beta_0 + \beta_1 \cdot x))^2. \tag{28}$$

Taking the first-order derivative of Eqn. 28 about the coefficients β_0, β_1 and equating it to 0, it is straightforward to obtain

$$\hat{\beta}_1 = \frac{\sum_{i=1}^{n}(x_i - \bar{x})(y_i - \bar{y})}{\sum_{i=1}^{n}(x_i - \bar{x})^2} \tag{29}$$

. and

$$\hat{\beta}_0 = \bar{y} - \hat{\beta}_1 \bar{x}, \tag{30}$$

. where $\bar{x}$ and $\bar{y}$ are mean values of x and y respectively, and $\hat{\beta}_0$ and $\hat{\beta}_1$ are the estimates of β_0 and β_1, respectively.

Since the expected value of ϵ

$$E\Big[\epsilon\Big] = E\Big[Y - (\beta_0 + \beta_1 X)\Big] = 0, \tag{31}$$

from Eqn. 28, it is straightforward to obtain

$$E\left[\epsilon^2\right] = \sum_{i=1}^{n} (y - (\beta_0 + \beta_1 \cdot x))^2 / n. \tag{32}$$

Therefore, the standard deviation of ϵ is

$$\sigma_\epsilon = \sqrt{E\left[\epsilon^2\right] - \left(E\left[\epsilon\right]\right)^2} = \sqrt{\sum_{i=1}^{n} (y_i - (\beta_0 + \beta_1 \cdot x_i))^2 / n}, \tag{33}$$

which is actually of the format of the root mean squared error (RMSE).

The Eqn. 28 can be solved by many optimization method, such as Newton method, pattern search or ordinary LS (OLS) method within python. However, in this code, the aim is to avoid using prerequisite modules as much as possible, so Eqn. 29, 30, and 33 are included within the MAPOD code. It is important to note the expressions in these three equations, as they will be compared with those estimated from the maximum likelihood method, to prove that they are the same under this situation.

2.3.1.3 Maximum likelihood method

Now let's review the assumption made in linear regression:

1. The distribution of X is arbitrary.
2. If $X = x$, then $Y = \beta_0 + \beta_1 x + \epsilon$, for some coefficients, β_0 and β_1 and some random noise variable ϵ.
3. $\epsilon \sim \mathrm{N}(0,\sigma_\epsilon^2)$ and is independent of X.
4. ϵ is independent across observations.

Based on these assumptions, the response Y is independent across observations, conditional on the predictor X. Besides, the noise variable ϵ has zero mean and constant variance, and follows the Normal distribution. Therefore, the conditional probability density function of Y for each x, given arbitrary number of data sets, (x_1, y_1), (x_2, y_2), ..., (x_n, y_n), can be written as

$$\prod_{i=1}^{n} p(y_i|x_i;\beta_0,\beta_1,\sigma_\epsilon^2) = \prod_{i=1}^{n} \frac{1}{\sqrt{2\pi\sigma_\epsilon^2}} e^{-\frac{(y_i-(\beta_0+\beta_1\cdot x_i))^2}{2\sigma_\epsilon^2}}. \tag{34}$$

For any estimates on unknown parameters, β_0, β_1, and ϵ, the pdf becomes

$$\prod_{i=1}^{n} p(y_i|x_i;\hat{\beta}_0,\hat{\beta}_1,\hat{\sigma}_\epsilon^2) = \prod_{i=1}^{n} \frac{1}{\sqrt{2\pi\hat{\sigma}_\epsilon^2}} e^{-\frac{(y_i-(\hat{\beta}_0+\hat{\beta}_1\cdot x_i))^2}{2\hat{\sigma}_\epsilon^2}}. \tag{35}$$

which is called likelihood, a function of the parameter values. For the convenience of calculation, usually it is taken as log-likelihood,

$$L(\hat{\beta}_0,\hat{\beta}_1,\hat{\sigma}_\epsilon^2) = log \prod_{i=1}^{n} p(y_i|x_i;\hat{\beta}_0,\hat{\beta}_1,\hat{\sigma}_\epsilon^2), \tag{36}$$

and so,

$$L(\hat{\beta}_0, \hat{\beta}_1, \hat{\sigma}_\epsilon^2) = -\frac{n}{2} log 2\pi - n log \hat{\sigma}_\epsilon - \frac{1}{2\hat{\sigma}_\epsilon^2} \sum_{i=1}^{n} (y - (\hat{\beta}_0 + \hat{\beta}_1 \cdot x))^2. \tag{37}$$

We can maximize Eqn. 37 to get the best estimates on unknowns. This method is called maximum likelihood [78]. Any optimization method can be used to maximize Eqn. 37, like those mentioned above for the least squares method. Taking the first-order derivative of Eqn. 37 and setting it as 0, to obtain

$$\hat{\beta}_1 = \frac{\sum_{i=1}^{n}(x_i - \bar{x})(y_i - \bar{y})}{\sum_{i=1}^{n}(x_i - \bar{x})^2}, \tag{38}$$

$$\hat{\beta}_0 = \bar{y} - \hat{\beta}_1 \bar{x}, \tag{39}$$

$$\sigma_\epsilon = \sqrt{\sum_{i=1}^{n} (y_i - (\beta_0 + \beta_1 \cdot x_i))^2 / n}. \tag{40}$$

It is obvious that the estimation equations above are the same as in Eqn. 29, 30, and 33. Therefore, in this framework, the numerical expression of unknown parameters are coded up directly, without having to claim which method it comes from. The authors prefer the maximum likelihood method, because it is more convenient and straightforward to compute the Fisher information matrix and apply the Wald method for confidence intervals on the "$\hat{a}$ vs. a" plots and POD curves. More details on this type of confidence interval calculation are given in Section 2.3.1.

2.3.2 "$\hat{a}$ vs. a" regression based POD

For signal response data, a lot more information is supplied in the signal for analysis than is in the hit/miss data. Here, the POD function is generated from the correlation of the "$\hat{a}$ vs. a" data [8, 9]. And through reviews on experiments data, it shows a log-log scale between $\hat{a}$ vs. a is given by:

$$ln\hat{a} = \beta_0 + \beta_1 ln a + \epsilon, \tag{41}$$

where the coefficients β_0 and β_1 can be determined by the maximum likelihood method, and the ϵ has a Normal distribution with zero mean and standard deviation σ_ϵ, $N(0, \sigma_\epsilon)$. This standard deviation can be determined by the residuals of the observed data, as shown in Section 2.3.1.

2.3.3 POD

The POD can be obtained as the probability that the obtained signal lies above arbitrary user-defined threshold:

$$POD(a) = 1 - \Phi\left[\frac{ln\hat{a}_{threshold} - (\beta_0 + \beta_1 ln a)}{\sigma_\epsilon}\right], \tag{42}$$

where Φ is the standard normal distribution function.

From Eqn. 42, it is straightforward to obtain:

$$POD(a) = \Phi\left[\frac{lna - \frac{ln\hat{a}_{threshold} - \beta_0}{\beta_1}}{\frac{\sigma_\epsilon}{\beta_1}}\right], \tag{43}$$

which is a cumulative log-normal distribution function with mean μ and standard deviation σ given by:

$$\mu = \frac{ln\hat{a}_{threshold} - \beta_0}{\beta_1}, \tag{44}$$

$$\sigma = \frac{\sigma_\epsilon}{\beta_1}, \tag{45}$$

where the parameters β_0, β_1, and σ_ϵ can be obtained by least squares method, maximum likelihood method or the numerical expression discussed in Section 2.3.1.

2.3.4 Confidence interval

In statistics, especially when uncertainty exists in physical systems, it is impossible to specify a discrete value to a variable with 100% certainty. Therefore instead of specifying a discrete value, it is given by a distribution. This distribution requires a confidence interval, which is given by:

$$P(a_{lower} \leq a \leq a_{upper}) = const, \tag{46}$$

where the const is the "confidence level", a_{lower} is called the "lower confidence limit" and a_{upper} is called the "upper confidence limit". The interval within a_{lower} and a_{upper} is called a "confidence interval" [27, 31]. Note, in POD calculations, only the lower confidence limit is used. If the confidence level is set as 95%, this implies that there is a 95% probability that this confidence interval contains the true population mean. The a_{lower} and a_{upper} depend on the sampled set and hence varies for each random set. These limits are typically calculated by drawing large number of samples from a given population.

In POD calculations, the probability of detecting a given defect size is set to 90% and is written as a_{90}. To account for the uncertainty, the upper bounds of 95% confidence interval is considered, which is written as $a_{90/95}$. Note, that these two values are not characteristic properties of a NDT system, but rather are calculated from the particular random results.

There are various methods, such as bootstrap, Wald method, and likelihood ratio method, used for confidence interval calculations. In current version of the framework, the Wald method is used. The Fisher information is required by the Wald method and in described in the section below.

2.3.4.1 Fisher information

In mathematical statistics, Fisher information [79] is used for measuring the amount of information that an observable random variable X carries about an unknown parameter θ of a distribution that models X. Formally, it is the expected value of the observed information. Observed information is the negative of the second derivative, the Hessian matrix, of the "log-likelihood" (the logarithm of the likelihood function).

Suppose that we observe random variables, X_1, X_2, ..., X_n, independently and identically distributed with density $f(X;\boldsymbol{\theta})$, where $\boldsymbol{\theta}$ is assumed to be a n-dimensional vector. The log-likelihood of the parameters $\boldsymbol{\theta}$ given the data X_1, X_2, ..., X_n is

$$l(\boldsymbol{\theta}|X_1, X_2, ..., X_n) = \sum_{i=1}^{n} log\, f(X_i|\boldsymbol{\theta}). \tag{47}$$

Then the observed information matrix can be obtained as

$$J(\boldsymbol{\theta}) = -\begin{pmatrix} \frac{\partial^2}{\partial\theta_1^2} & \frac{\partial^2}{\partial\theta_1\partial\theta_2} & \cdots & \frac{\partial^2}{\partial\theta_1\partial\theta_n} \\ \frac{\partial^2}{\partial\theta_2\partial\theta_1} & \frac{\partial}{\partial\theta_2} & \cdots & \frac{\partial^2}{\partial\theta_2\partial\theta_n} \\ \cdots & \cdots & \cdots & \cdots \\ \frac{\partial^2}{\partial\theta_n\partial\theta_1} & \frac{\partial^2}{\partial\theta_n\partial\theta_2} & \cdots & \frac{\partial^2}{\partial\theta_n^2} \end{pmatrix} l(\boldsymbol{\theta}). \tag{48}$$

With observed information matrix ready, the Fisher information can be obtained as

$$I(\boldsymbol{\theta}) = E(J(\boldsymbol{\theta})). \tag{49}$$

2.3.4.2 Wald method

Wald method [80, 81] is a well-known likelihood-based procedure for calculating confidence interval, and usually performs well in large samples. For a location-scale distribution or for a distribution which can be transformed to a location-scale distribution, the Wald confidence interval is easy to compute for quantiles. Therefore, it is suitable for exponential, Weilbull, and lognormal distributions. The MH1823 [27], the officially used POD software from the department of defense (DOD), United State, also utilizes this method for calculation of confidence interval.

The Lawless' general procedure for a location-scale distribution is used for calculating the confidence intervals using Wald method. Let x_p be the quantile of a location-scale distribution with parameter u and b respectively, while w_p is the quantile of the same distribution with $u = 0$, and $b = 1$. Then, $x_p = u + w_p b$ which we can estimate by

$$\hat{x}_p = \hat{u} + w_p \hat{b}, \tag{50}$$

using maximum likelihood (ML) estimates $\hat{u}$ and $\hat{b}$. The pivotal quantity is

$$Z_p = \frac{\hat{x}_p - x_p}{se(\hat{x}_p)}, \tag{51}$$

where

$$se(\hat{x}_p) = \left(var(\hat{u}) + w_p^2 var(\hat{b}) + 2 w_p cov(\hat{u}, \hat{b}) \right)^{1/2}, \tag{52}$$

where the variance and covariance terms come from the asymptotic covariance matrix for $(\hat{u}, \hat{b})$, which is the inverse of the Fisher's observed information matrix [79], $I(\hat{u}, \hat{b})$, evaluated at $(\hat{u}, \hat{b})$. The diagonal elements of $(I(\hat{u}, \hat{b}))^{-1}$ give the variances and the off-diagonal elements give the covariance.

Due to the assumption of asymptotic normality of maximum likelihood estimates, Z_p is approximately $N(0,1)$. Let Z be a $N(0,1)$ random variable and z_α be the value such that

$$P(Z < z_\alpha) = \alpha. \tag{53}$$

A Wald $100(1-\alpha)\%$ CI for x_p is given by

$$\left(\hat{x}_p + z_{\frac{\alpha}{2}} se(\hat{x}_p), \hat{x}_p - z_{\frac{\alpha}{2}} se(\hat{x}_p) \right). \tag{54}$$

2.3.4.3 Application on "$\hat{a}$ vs. a" regression and POD curves

As mentioned in [8, 9], the "$\hat{a}$ vs. a" regression is constructed with a regression line (solid black line), surrounded by two sets of nearly parallel bounds (dashed blue lines), as shown in Fig. 7

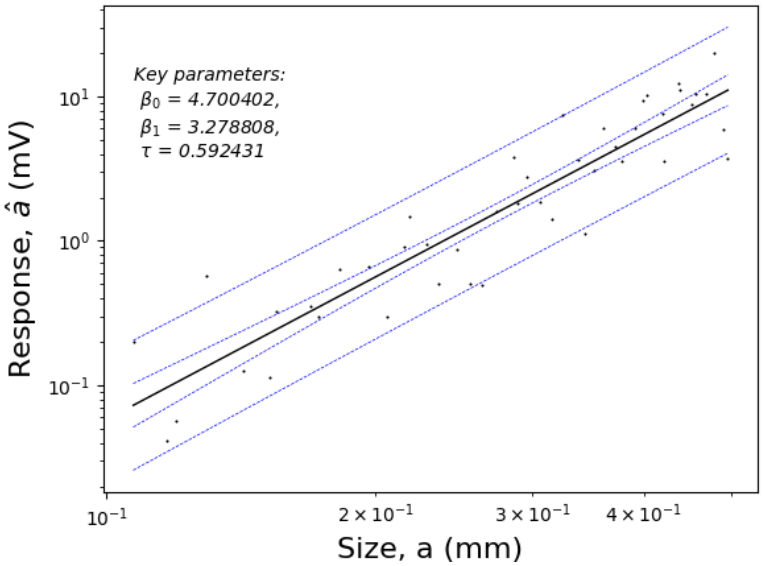

Figure 7: "$\hat{a}$ vs. a" regression, within bounded lines.

The innermost set is the 95% confidence bounds on the line itself. The outer set of dashed lines is called the 95% prediction bounds. A new response value is expected to be contained by these bounds in 95 of 100 similar situations. Usually these sets of lines go further at both ends, meaning less confidence in the solid line as we get further from the centroid of the data. For linear regression problem, we obtain the estimates on the intercept and slope of the solid line along with uncertainties on those estimates. Near the centroid the uncertainty in the slope has little influence, but becomes increasingly influential away from the centroid, resulting in a "dog-bone" confidence bounds.

The estimated response, $\hat{y}$, is given by the regression equation

$$\hat{y} = \hat{\beta}_0 + \hat{\beta}_1 \cdot x. \tag{55}$$

Based on the variance of a sum, the variance on $\hat{y}$ can be expressed as

$$var(\hat{y}) = var(\hat{\beta}_0 + \hat{\beta}_1 \cdot x) = var(\hat{\beta}_0) + 2xcov(\hat{\beta}_0, \hat{\beta}_1) + x^2 var(\hat{\beta}_1), \tag{56}$$

from which the 95% Wald confidence bounds on $\hat{y}$ can be constructed as

$$\hat{y}_{\alpha=0.95} = \hat{y} \pm 1.645 se_{\hat{y}} = \hat{\beta}_0 + \hat{\beta}_1 x \pm 1.645\sqrt{var(\hat{y})}. \tag{57}$$

The 95% prediction bounds can be constructed following the same process, except that the variance of the random residual also needs to be included

$$var_{total}(\hat{y}) = var(\hat{y}) + \sigma_\epsilon^2. \tag{58}$$

The variances and covariance terms in Eqn. 56 can be obtained from the inverse matrix of the Fisher information. The distribution of model response, y, has the same format of Eqn. 34, and the corresponding log-likelihood follows Eqn. 37. Thus, the resulting Fisher information matrix is

$$I\left(\hat{\beta}_0, \hat{\beta}_1, \hat{\sigma}_\epsilon\right) = \begin{pmatrix} \frac{n}{\hat{\sigma}_\epsilon^2} & \frac{\sum_{i=1}^n X_i}{\hat{\sigma}_\epsilon^2} & 0 \\ \frac{\sum_{i=1}^n X_i}{\hat{\sigma}_\epsilon^2} & \frac{\sum_{i=1}^n X_i^2}{\hat{\sigma}_\epsilon^2} & 0 \\ 0 & 0 & \frac{2n}{\hat{\sigma}_\epsilon} \end{pmatrix}, \tag{59}$$

then the covariance matrix has the format

$$Var\left(\hat{\beta}_0, \hat{\beta}_1, \hat{\sigma}_\epsilon\right) = \begin{pmatrix} V_{00} & V_{01} & V_{02} \\ V_{10} & V_{11} & V_{12} \\ V_{20} & V_{21} & V_{22} \end{pmatrix}. \tag{60}$$

When applying the Wald method to POD curves, the covariance matrix on $\hat{\mu}$ and $\hat{\sigma}$ is can be calculated from Eqn. 60

$$Var\left(\hat{\mu},\hat{\sigma}\right)=\begin{pmatrix}\frac{1}{\hat{\beta}_1^2}\left[V_{00}+2\hat{\mu}V_{01}+\hat{\mu}^2V_{11}\right] & \frac{1}{\hat{\beta}_1^2}\left[\hat{\sigma}V_{01}-V_{20}-\hat{\mu}V_{12}+\hat{\mu}\hat{\sigma}V_{11}\right]\\ \frac{1}{\hat{\beta}_1^2}\left[\hat{\sigma}V_{01}-V_{20}-\hat{\mu}V_{12}+\hat{\mu}\hat{\sigma}V_{11}\right] & \frac{1}{\hat{\beta}_1^2}\left[V_{22}-2\hat{\sigma}V_{21}+\hat{\sigma}^2V_{11}\right]\end{pmatrix}. \tag{61}$$

With this information ready, it is still not straightforward because the POD curve is actually a curriculum density function with a log-normal distribution, which is not a location-scale distribution. However, the log format of the random variable follows the normal distribution. Therefore, the lower confidence interval on this corresponding normal distribution, $N(\hat{\mu},\hat{\sigma})$, can be generated. Due to the monotone characteristics of log-normal distribution [82, 83], the exponential value of the results can be calculated.

2.4 Sensitivity Analysis

Sensitivity analysis is used to determine how the model response is affected by the random input parameters. In this framework, the variance-based SA, called Sobol indices [42, 43, 84], is used.

$M(\mathbf{X}) = f(\mathbf{X})$ represented from a black-box perspective, where $\mathbf{X}$ is a vector containing m random variables, can be decomposed as [84]

$$\begin{aligned}M(\mathbf{X}) =& f_0+\sum_{i=1}^{m}f_i(X_i)+\sum_{i<j}^{m}f_{i,j}(X_i,X_j)\\ &+\ldots+f_{1,2,\ldots,m}(X_1,X_2,\ldots,X_m),\end{aligned} \tag{62}$$

with f_0 being a constant and f_i being a function of X_i. All the terms in the functional decomposition are orthogonal, which leads to the decomposition in terms of the conditional expected values

$$f_0=(M(\mathbf{X})), \tag{63}$$

$$f_i(X_i)=(M(\mathbf{X})|X_i)-f_0, \tag{64}$$

$$f_{i,j}(X_i,X_j)=(M|X_i,X_j)-f_0-f_i(X_i)-f_j(X_j), \tag{65}$$

and so on. This can be further simplified in order to obtain the decomposition of the variance expression [48]

$$\mathrm{ar}(M(\mathbf{X}))=\sum_{i=1}^{m}V_i+\sum_{i<j}^{m}V_{i,j}+\ldots+V_{1,2,\ldots,m}, \tag{66}$$

where

$$V_i=\mathrm{ar}_{X_i}(\mathbf{X}_{\sim i}(M(\mathbf{X})|X_i)), \tag{67}$$

$$V_{i,j}=\mathrm{ar}_{X_{i,j}}(\mathbf{X}_{\sim i,j}(M(\mathbf{X})|X_i,X_j))-V_i-V_j, \tag{68}$$

and so on. The set of all variables except X_i is denoted by $\mathbf{X}_{\sim i}$.

The first-order Sobol indices, also known as the "main effect index", is written as

$$S_i = \frac{V_i}{\mathrm{ar}(M(\mathbf{X}))}, \tag{69}$$

The total-effect Sobol indices, also known as the "total-order index", is given by

$$\begin{aligned} S_{T_i} &= \frac{\mathbf{x}_{\sim i}(\mathrm{ar}_{X_i}(M(\mathbf{X})|\mathbf{X}_{\sim i}))}{\mathrm{ar}(M(\mathbf{X}))} \\ &= 1 - \frac{\mathrm{ar}_{\mathbf{X}_{\sim i}}(_{X_i}(M(\mathbf{X})|\mathbf{X}_{\sim i}))}{\mathrm{ar}(M(\mathbf{X}))}, \end{aligned} \tag{70}$$

The Monte Carlo sampling method is used to estimate the Sobol indices [48]. This involves generating a sequence of randomly distributed points for the MCS. The low-discrepancy sequences commonly used in SA include the Sobol sequence and the Latin Hypercube design. The procedure is summarized as follows:

1. Generate a $N \times 2m$ sample matrix, where N represents a row of a sample point in the hyperspace of $2m$ dimensions. This is done with respect to the probability distributions of the input variables.
2. The first m columns of the matrix is used for matrix **A**, while the remaining m columns is used for matrix **B**. Therefore, two independent samples of N points in the m-dimensional unit hypercube is generated.
3. Build another m matrices of dimensions $N \times m$. This is done by replacing the i^{th} column of the **B** matrix with the i^{th} column of the **A** matrix, given by $\mathbf{AB}_i$, for $i = 1, 2, ..., m$.
4. $N(m+2)$ points in the input space (one for each row) is specified in total by the **A**, **B**, and the m $\mathbf{AB}_i$ matrices. The model responses $\mathbf{f}(\mathbf{A})$, $\mathbf{f}(\mathbf{B})$ and $\mathbf{f}(\mathbf{AB})$ correspond to the evaluation of the model at the design point in the **A**, **B**, and **AB** matrices.
5. The sensitivity indices are calculated using the estimators below. First-order and total-order Sobol indices can be obtained using the Monte Carlo estimators [48, 85], given by

$$\begin{aligned} &\mathrm{ar}_{X_i}(_{\mathbf{X}_{\sim i}}(M(\mathbf{X})|X_i)) \\ &\approx \frac{1}{N}\sum_{j=1}^{N} \mathbf{f}(\mathbf{B})_j(\mathbf{f}(\mathbf{AB}_i)_j - \mathbf{f}(\mathbf{A})_j), \end{aligned} \tag{71}$$

and

$$\begin{aligned} &\mathbf{x}_{\sim i}(\mathrm{ar}_{X_i}(M(\mathbf{X})|\mathbf{X}_{\sim i})) \\ &\approx \frac{1}{2N}\sum_{j=1}^{N} (\mathbf{f}(\mathbf{A})_j - \mathbf{f}(\mathbf{AB}_i)_j)^2. \end{aligned} \tag{72}$$

3 NUMERICAL VALIDATION

3.1 Case 1: Spherical void defect

3.1.1 Problem description

The ultrasonic benchmark case, called spherically-void-defect case, developed by the World Federal Nondestructive Evaluation Center in 2004 is described in this section. The experimental setup and validation of the physics based simulation model is shown in Fig. 8. The spherically void defect, whose radius is 0.34 mm, is included in a fused quartz block, which is surrounded by water. A spherically focused transducer, the radius of which is 6.23mm, is used to detect this defect. The frequency range is set to be [0, 10MHz].

The analytical model used in this work is known as the Thompson-Gray model. This model is based on the paraxial approximation of the incident and scattered ultrasonic waves, computing the spectrum of voltage at the receiving transducer in terms of the velocity diffraction coefficients of the transmitting/receiving transducers, scattering amplitude of the defect and a frequency-dependent coefficient known as the system-efficiency function. In this work, velocity diffraction coefficients were calculated using the multi-Gaussian beam model and scattering amplitude of the spherical-void was calculated using the method of separation of variables. The system efficiency function, which is a function of the properties and settings of the transducers and the pulser, was taken from the WFNDEC archives. The time-domain pulse-echo waveforms are computed by performing Fast Fourier Transforms (FFT) on the voltage spectrum. The foregoing system model was shown to be very accurate in predicting pulse-echo from the spherical void if the paraxial approximation is satisfied and radius of the void is small. To guarantee the effectiveness of this analytical model on the benchmark problem mentioned above, it is validated on this case with experimental data, given in Fig. 8 , which shows that

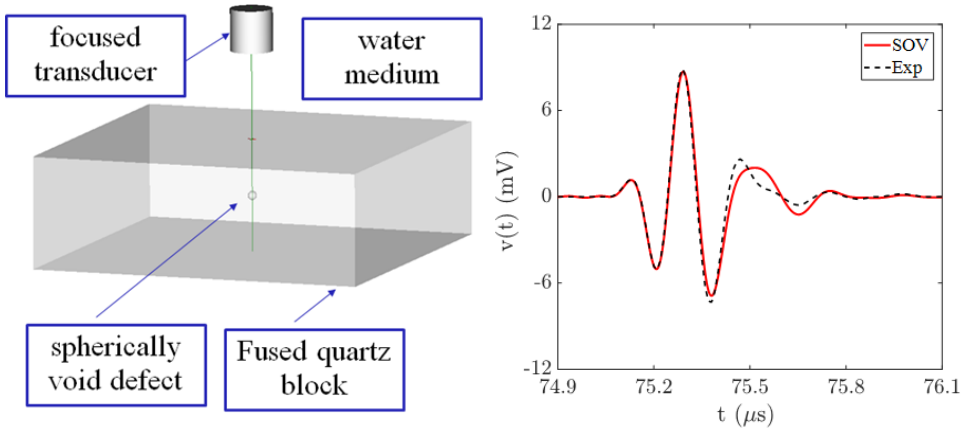

Figure 8: Setup of the spherically-void-defect benchmark case (left) and results of comparison between experimental data (Exp) and the analytical solution (SOV).

the results match well.

For the POD calculation, three uncertainty parameters for the original problem are set: the probe angle of transducer ~ $N(0deg, 0.5deg)$; the F number of the frequency ~ $U(13,15)$; and the x location of transducer ~ $U(0mm, 1mm)$. Simulations will be run at the defect sizes: 0.1mm, 0.2mm, 0.3mm, 0.4mm and 0.5mm respectively for the data collection before the POD calculation. The detection threshold is set to 6.5mV.

3.1.2 Results

Results on "$\hat{a}$ vs. a" regression are shown in Fig. 9 and the related results of the POD are shown in Fig. 10. Figures 9a and 10a are generated directly from the input data without constructing the metamodel. Figures 9b and 10b are the same plots, but first the PC-Kriging metamodel is constructed

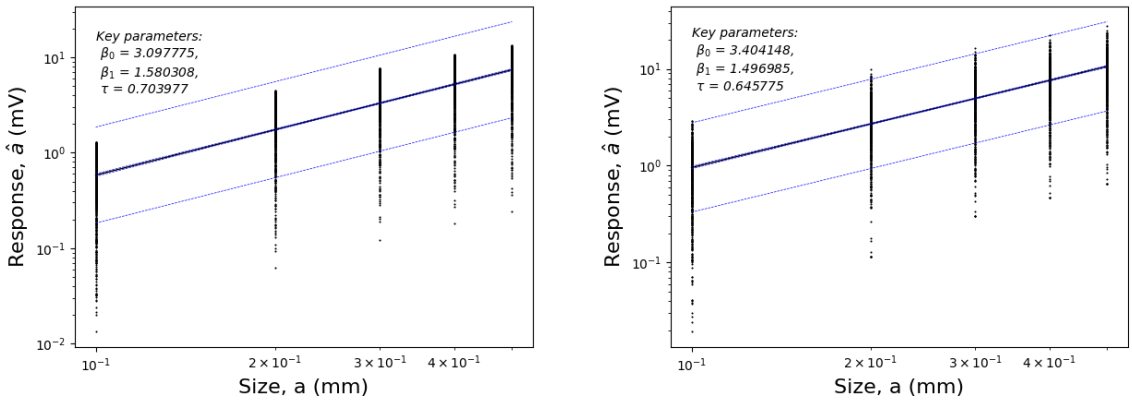

(a) No metamodel. **(b)** PC-Kriging.

Figure 9: "$\hat{a}$ vs. a" plot.

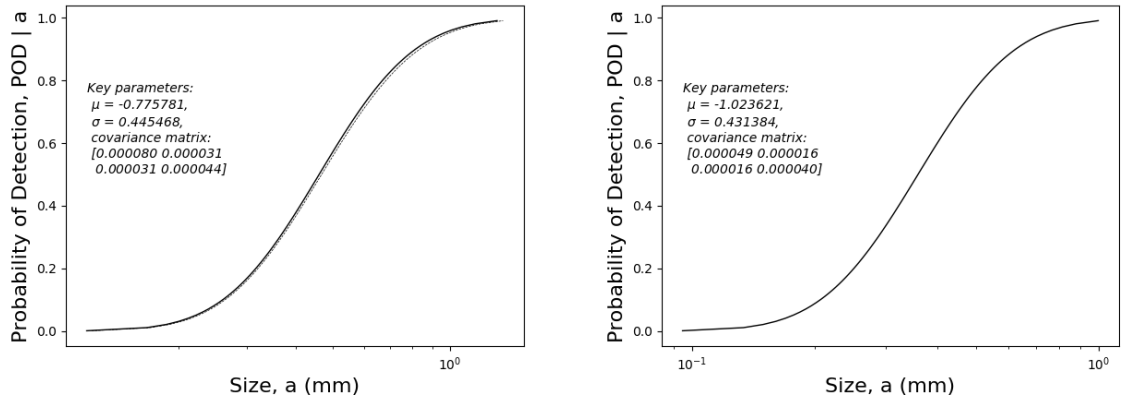

(a) No metamodel. **(b)** PC-Kriging.

Figure 10: POD curves.

Table 1: Parameter comparison between MH1823 and pyMAPOD.

Parameter	MH1823	pyMAPOD (no metamodel)	pyMAPOD (PC-Kriging)
β_0	3.0978	3.0978	3.4041
β_1	1.5803	1.5803	1.4970
τ	0.7040	0.7040	0.6458
μ	-0.7758	-0.7758	-1.0236
σ	0.4455	0.4455	0.4314

using data from the physics-based simulation model. The metamodel is then used to generate the "$\hat{a}$ vs. a" plot and the POD curves. 1000 training points for each defect size is used to construct the POD curve in the case where the metamodel isn't constructed compared to only 120 point per defect size in the case where the metamodel is constructed. These results have also been compared to those generated by the MH1823 [32] software. The key parameters, such as β_0, β_1, and τ in the "$\hat{a}$ vs. a" plots and μ, σ in the corresponding covariance matrix in the POD curves, are shown in Table 1. The results for the case where the metamodel is not constructed matches the MH1823 results extremely well, while the PC-Kriging metamodeling results do not match. In order to improve these results, the number of training data sets used to construct the metamodel will need to be increased. The current metamodel has an RMSE of 0.7mV and below for all the defect sizes, with a high $\sigma_{testing}$ (> 100%).

REFERENCES

[1] P. Cawley, "Non-Destructive Testing - Current Capabilities and Future Directions," *Journal of Materials: Design and Applications*, vol. 215, pp. 213–223, 2001.

[2] Y. Zhu, G. Tian, R. Lu, and H. Zhang, "A Riview of Optical NDT Technologies," *Sensors*, vol. 11, pp. 7773–7798, 2011.

[3] S. Verma, S. Bhadauria, and S. Akhtar, "Review of Nondestructive Testing Methods for Condition Monitoring of Concrete Structures," *Journal of Construction Engineering*, vol. 2013, pp. 1–11, 2013.

[4] P. Kah, B. Mvola, J. Martikainen, and R. Suoranta, "Real Time Non-Destructive Testing Methods of Welding," *Advanced Materials Research*, vol. 933, pp. 109–116, 2014.

[5] L. Pazdera, L. Topolar, J. Smutny, and K. Timcakova, "Nondestructive Testing of Advanced Concrete Structure During Lifetime," *Advances in Materials Science and Engineering*, vol. 2015, pp. 1–5, 2015.

[6] R. B. Thompson and T. A. Gray, "A Model Relating Ultrasonic Scattering Measurements Through Liquid - Solid Interfaces to Unbounded Medium Scattering Amplitudes," *The Journal of the Acoustical Society of America*, vol. 74, no. 4, pp. 1279–1290, 1983.

[7] J. Gao, K. Wang, and J. Sun, "Study on the Technology of Ultrasonic Imaging Detection Based on Phase Array," *Image Processing and Pattern Recognition*, vol. 6, pp. 71–78, 2013.

[8] P. Mares, "Simulation as a Support for Ultrasonic Testing," *Journal of Modern Physics*, vol. 5, pp. 1167–1172, 2014.

[9] F. Liu, C. Xu, Y. He, D. Xiao, F. Meng, Z. Xiao, and Q. Pan, "Research on the Ultrasonic Test System for the Complex Curved Surface Based on Robot," *2015 IEEE Far East NDT New Technology and Application Forum (FENDT)*, pp. 173–176, 2015.

[10] X.-L. Yan, S.-Y. Dong, B.-S. Xu, and Y. Gao, "Progress and Challenges of Ultrasonic Testing for Stress in Remanufacturing Laser Cladding Coating," *Materials*, vol. 11, pp. 1–16, 2018.

[11] C. M. Silva, P. A. Rosa, A. G. Atkins, and P. A. Martins, "An Electromagnetic Testing Machine for Determining Fracture Toughness under Different Loading Rate and Superimposed Pressure," *Journal of Strain Analysis*, vol. 2014, pp. 437–444, 2014.

[12] P. Gao, C. Wang, Y. Li, and Z. Cong, "Electromagnetic and Eddy Current NDT in Weld Inspection: A Review," *Insight - Non-Destructive Testing and Condition Monitoring*, vol. 2015, pp. 337–345, 2015.

[13] S. Liu, Y. Sun, M. Gu, C. Liu, L. He, and Y. Kang, "Review and Analysis of Three Representative Electromagnetic NDT methods," *Insight - Non-Destructive Testing and Condition Monitoring*, vol. 59, pp. 176–183, 2017.

[14] Z. Cai, H. Cheng, and C. Liu, "Nonlinear Electromagnetic Acoustic Testing Method for Tensile Damage Evaluation," *Journal of Sensors*, vol. 2018, pp. 1–11, 2018.

[15] S.-N. Choi, S.-Y. Hong, and W.-G. Hwang, "Performance Demonstration for an Automated Ultrasonic Testing System for Piping Welds," *Journal of Nuclear Sience and Technology*, vol. 49, pp. 562–570, 2012.

[16] O. Martin, M. Pereda, J. Santos, and J. Galan, "Assessment of Resistance Spot Welding Quality Based on Ultrasonic Testing and Tree-Based Techniques," *Journal of Materials Processing Technology*, vol. 214, pp. 2478–2487, 2014.

[17] K. Manjula, K. Vijayarekha, and B. Venkatraman, "Weld Flaw Detection Using Various Ultrasonic Techniques: A Review," *Journal of Applied Sciences*, vol. 14, pp. 1529–1535, 2014.

[18] K. Adamus and P. Lacki, "Assessment of Aluminum FSW Joints Using Ultrasonic Testing," *Archives of Metallurgy and Materials*, vol. 62, pp. 2399–2404, 2017.

[19] A. Poudel, J. Strycek, and T. P. Chu, "Air-Coupled Ultrasonic Testing of Carbon-Carbon Composite Aircraft Brake Disks," *Materials Evaluation*, vol. 71, pp. 987–994, 2013.

[20] B. Masserey, C. Raemy, and P. Fromme, "High-Frequency Guided Ultrasonic Waves for Hidden Defect Detect in Multi-Layered Aircraft Structures," *Ultrasonics*, vol. 54, pp. 1720–1728, 2014.

[21] M. Carpriotti, H. Kim, F. Scalea, and H. Kim, "Non-Destructive Inspection of Impact Damage in Composite Aircraft Panels by Ultrasonic Guided Waves and Statistical Processing," *Materials*, vol. 10, pp. 1–12, 2017.

[22] G. Boopathy, G. Surrendar, and A. Nema, "Review on Non-Destructive Testing of Composite Materials in Aircraft Applications," *International Journal of Mechanical Engineering and Technology (IJMET)*, vol. 8, pp. 1334–1342, 2017.

[23] X. Wang, P. W. Tse, C. K. Mechefske, and M. Hua, "Experimental Investigation of Reflection in Guided Wave-Based Inspection for the Characterization of Pipeline Defects," *NDT/E International*, vol. 43, pp. 365–374, 2010.

[24] K. Sudheera and N. M. Nandhitha, "Application of Hilbert Transform for Flaw Characterization in Ultrasonic Signals," *Indian Journal of Science and Technology*, vol. 8, pp. 1–6, 2015.

[25] A. Ahmed, K. S. Badarinarayan, N. A. R., and G. G., "Development of Ultrasonic Reference Standards for Defect Characterization in Carbon Fiber Composites," *International Research Journal of Engineering and Technology (IRJET)*, vol. 2, pp. 840–844, 2015.

[26] L. Bai, A. Velichko, and B. W. Drinkwater, "Ultrasonic Defect Characterization - Use of Amplitude, Phase and Frequency Information," *The Journal of the Acoustic Society of America*, vol. 143, pp. 349–360, 2018.

[27] "Nondestructive Evaluation System Reliability Assessment," *MIL-HDBK-1823, Department of Defense Handbook, Wright-Patterson AFB, USA*, 1999.

[28] A. P. Berens, W. Hoppe, D. A. Stubbs, and O. Scott, "Probability of Detection (POD) Analysis for the Advanced Retirement for Cause (RFC)/Engine Structural Integrity Program (ENSIP) Nondestructive Evaluation (NDE) System Development," *Material Correlation Study*, vol. 3, pp. 1–32, 2001.

[29] G. A. Georgiou, "Probability of Detection (PoD) Curves. Derivation, Application and Limitations," *Jacobi Consulting Limited*, vol. 454, 2006.

[30] J. H. Kurz, S. Dugan, and A. Jungert, "Reliability Considerations of NDT by Probability of Detection (POD) Determination Using Ultrasound Phased Array - Results from a Project in Frame of the German Nuclear Safety Research Program," *5th European-American Workshop on Reliability of NDE*, vol. 16, pp. 1–11, 2013.

[31] "Nondestructive Evaluation System Reliability Assessment," *MIL-HDBK-1823A, Department of Defense Handbook, Wright-Patterson AFB, USA*, 2009.

[32] C. Annis, "Statistical Best-Practices for Building Probability of Detection (POD) Models," *R Package MH1823, Version 2.5, http://www.statisticalengineering.com/mh1823/mh1823-algorithms.html*, 2010.

[33] L. Lilburne and S. Tarantola, "Sensitivity Analysis of Spatial Models," *International Journal of Geographical Information Science*, vol. 23, pp. 151–168, 2009.

[34] A. Charzynska, A. Natecz, M. Rybinski, and A. Gambin, "Sensitivity Analysis of Mathematical Models of Signaling Pathways," *Journal of Biotechnology, Computational Biology and Bionanotechnology*, vol. 93, pp. 291–308, 2012.

[35] R. H. D. Staelen and K. Beddek, "Sensitivity Analysis and Variance Reduction in a Stochastic NDT Problem," *International Journal of Computer Mathematics*, vol. 92, pp. 1874–1882, 2015.

[36] F. Ferretti, A. Saltelli, and S. Tarantola, "Trends in Sensitivity Analysis Practice in the Last Decades," *Science of the Total Environment*, vol. 568, pp. 666–670, 2016.

[37] E. Borgonovo and E. Plischke, "Sensitivity Analysis: A Review of Recent Advances," *European Journal of Operational Research*, vol. 248, pp. 869–887, 2016.

[38] E. Castillos, A. Conejo, R. Minguez, and C. Castillo, "A Closed Formula for Local Sensitivity Analysis in Mathematical Programming," *Engineering Optimization*, vol. 38, pp. 93–112, 2007.

[39] A. Sher, K. Wang, A. Wathen, P. Maybank, G. Mirams, D. Abramson, D. Noble, and D. Gavaghan, "A Local Sensitivity Analysis Method for Developing Biological Models with Identifiable Parameters: Application to Cardiac Ionic Channel Modelling," *Future Generation Computer System*, vol. 29, pp. 591–598, 2011.

[40] B. Iooss and A. Saltelli, "Introduction to Sensitivity Analysis," *Springer International Publishing, Switzerland, 2015*, 2015.

[41] X. Zhou and H. Lin, "Local Sensitivity Analysis," *Encyclopedia of GIS*, pp. 1116–1119, 2017.

[42] I. Sobol' and S. Kuchereko, "Sensitivity Estimates for Nonlinear Mathematical Models," *Mathematical Modelling and Computational Experiments*, vol. 1, pp. 407–414, 1993.

[43] I. Sobol', "A Primer for the Monte Carlo Method," *Boca Raton CRC Press*, 1994.

[44] T. Homma and A. Saltelli, "Importance Measures in Global Sensitivity Analysis of Nonlinear Models," *Reliability Engineering and System Safety*, vol. 52, pp. 1–17, 1996.

[45] A. Saltelli, "Making Best Use of Model Evaluation to Compute Sensitivity Indices," *Computer Physics Communication*, vol. 145, pp. 280–297, 2002.

[46] J. W. Hall, "Uncertainty-Based Sensitivity Indices for Imprecise Probability Distribution," *Reliability Engineering and System Safety*, vol. 91, pp. 1443–1451, 2006.

[47] J. Morio, "Global and Local Sensitivity Analysis Methods for a Physical System," *European Journal of Physics*, vol. 32, pp. 1–9, 2011.

[48] I. Sobol', "Global Sensitivity Indices for Nonlinear Mathematical Models and Their Monte Carlo Estimates," *Mathematics and Computers in Simulation*, vol. 55, pp. 271–280, 2001.

[49] A. B. Owen, "Sobol' Indices and Shapley Value," *SIAM/ASA Journal of Uncertainty Quantification*, vol. 2, pp. 245–251, 2014.

[50] G. Chastaing, C. Prieur, and F. Gamboa, "Generalized Sobol Sensitivity Analysis Indices for Dependent Variables: Numerical Methods," *Journal of Statistical Computation and Simulation*, vol. 85, pp. 1306–1333, 2015.

[51] R. Thompson, L. Brasche, D. Forsyth, E. Lindgren, and P. Swindell, "Recent Advances in Model-Assisted Probability of Detection," *4th European-American Workshop on Reliability of NDE, Berlin, Germany*, June 24-26, 2009.

[52] J. C. Aldrin, J. S. Knopp, E. Lindgren, and K. Jata, "Model-Assisted Probability of Detection Evaluation for Eddy Current Inspection of Fastener Sites," *Review of Quantitative Nondestructive Evaluation*, vol. 28, pp. 1784–1791, 2009.

[53] J. Blitz and G. Simpson, "Ultrasonic Methods of Non-destructive Testing," *London Chapman Hall*, 1996.

[54] J. Aldrin, E. Medina, E. Lindgren, C. Buynak, and J. Knopp, "Case Studies for Model-Assisted Probabilistic Reliability Assessment for Structural Health Monitoring Systems," *Review of Progress in Nondestructive Evaluation*, vol. 30, pp. 1589–1596, 2011.

[55] J. Aldrin, E. Medina, E. Lindgren, C. Buynak, G. Steffes, and M. Derriso, "Model-Assisted Probabilistic Reliability Assessment for Structure Health Monitoring Systems," *Review of Quantitative Nondestructive Evaluation*, vol. 29, pp. 1965–1972, 2010.

[56] S. J. Knopp, P. M. Blodgett, and C. A. Aldrin, "Efficient Propagation of Uncertainty in Simulations via the Probabilistic Collocation Method," *Studies in Applied Electromagnetic and Mechanics; Electromagnetic Nondestructive Evaluation Proceedings*, vol. 35, pp. 141 – 148, 2011.

[57] R. Miorelli, X. Artusi, B. A. Addessalem, and C. Reboud, "Database Generation and Exploitation for Efficient and Intensive Simulation Studies," *Review of Progress in Quantitative Nondestructive Evaluation*, vol. 1706, pp. 180 002–1–180 002–9, 2016.

[58] Z. Liu, W. Li, and M. Yang, "Two General Extension Algorithms of Latin Hypercube Sampling," *Mathematical Problems in Engineering*, vol. 2015, pp. 1–9, 2015.

[59] "Evaluation of Measurement Data, GUM Supplement 1 âĂŞ Propagation of Distributions Using a Monte Carlo Method," *Joint Committee for Guides in Metrology*, 2008.

[60] A. Shapiro, "Monte Carlo Sampling Methods," *Handbooks in Operations Research and Management Science*, vol. 10, pp. 353–425, 2003.

[61] M. D. Shields and J. Zhang, "The generalization of Latin Hypercube Sampling," $Reliability\ Engineering\ \&\ System\ Safety$, vol. 148, pp. 96–108, 2016.

[62] N. Wiener, "The Homogeneous Chaos," *American Journal of Mathematics*, vol. 60, pp. 897–936, 1938.

[63] Z. Zhang, T. El-Moselhy, I. Elfadel, and L. Daniel, "Calculation of Generalized Polynomial-Chaos Basis Functions and Gauss Quadrature Rules in Hierarchical Uncertainty Quantification," *IEEE Transactions on Computer-Aided Design of Integrated Circuits and Systems*, vol. 33, no. 5, pp. 728 – 740, 2014.

[64] G. Blatman, "Adaptive Sparse Polynomial Chaos Expansion for Uncertainty Propagation and Sensitivity Analysis," *Ph.D. Thesis, Blaise Pascal University - Clermont II. 3, 8, 9*, 2009.

[65] G. Blatman and B. Sudret, "An adaptive algorithm to build up sparse polynomial chaos expansions for stochastic finite element analysis," *Probabilistic Engineering Mechanics*, vol. 25, no. 2, pp. 183–197, 2010.

[66] G. Blatman and B. Sudret, "Adaptive sparse polynomial chaos expansion based on Least Angle Regression," *Journal of Computational Physics*, vol. 230, pp. 2345–2367, 2011.

[67] M. Udell, C. Horn, R. Zadeh, and S. Boyd, "Generalized Low Rank Models, Generalized Low Rank Models," *Foundations of Trends in Machine Learning*, vol. 9, no. 1, pp. 1–118, 2016.

[68] B. Efron, T. Hatie, I. Johnstone, and R. Tibshirani, "Least Angle Regression," *The Annals of Statistics*, vol. 32, no. 2, pp. 407–499, 2004.

[69] J. Sacks, W. Welch, J. T. Michell, and P. H. Wynn, "Design and Analysis of Computer Experiments," *Statistical Science*, vol. 4, pp. 409–423, 1989.

[70] J. I. A. Forrester, A. Sobester, and J. A. Keane, "Engineering Design via Surrogate Modelling: A Practical Guide," in *Engineering Design via Surrogate Modelling: A Practical Guide*, 2008, pp. 33–76.

[71] D. G. Krige, "A Statistical Approach to Some Basic Mine Valuation Problems on the Witwatersrand," *Journal of the Chemical, Metallurgical and Mining Engineering Society of South Africa*, vol. 52, no. 6, pp. 119–139, 1951.

[72] J. Ryu, K. Kim, T. Lee, and D. Choi, "Kriging Interpolation Methods in Geostatistics and DACE Model," *Korean Society of Mechanical Engineering International Journal*, vol. 16, no. 5, pp. 619–632, 2002.

[73] T. Gneiting, W. Kleiber, and M. Schlather, "Matern Cross-Covariance Functions for Multivariate Random Fields," *Journal of the American Statistical Association*, vol. 105, no. 491, pp. 1167–1177, 2010.

[74] R. Schobi, B. Sudret, and J. Wiart, "Polynomial-chaos-based Kriging," *International Journal of Uncertainty Quantification*, vol. 5, pp. 193–206, 2015.

[75] R. Schobi, B. Sudret, and S. Marelli, "Rare event estimation using Polynomial-Chaos-Kriging," *ASCE-ASME Journal of Risk and Uncertainty in Engineering Systems, Part A: Civil Engineering*, 2016.

[76] M. Kutner, C. Nachtsheim, J. Neter, and W. Li, "Applied Linear Statistical Models," *McGraw-Hill Irwin*, ISBN 0-07-238688-6.

[77] H. Abdi, "The method of least squares," *Encyclopedia of Measurement and Statistics*, 2007.

[78] C. Shalizi, "The Method of Maximum Likelihood for Simple Linear Regression," *Online course, Carnegie Mellon University*.

[79] B. Godo and A. Nagy, "Fisher Information and Topological Pressure ," *Journal of Mathematical Physics*, vol. 58, 2017.

[80] N. Dean and M. Pagano, "Evaluating Confidence Interval Methods for Binomial Proportions in Clustered Surveys," *Journal of Survey Statistics and Methodology*, vol. 3, no. 4, pp. 484–503, 2015.

[81] K. Aho and R. Bowyer, "Confidence Intervals for Ratios of Proportions: Implications for Selection Ratios," *Methods in Ecology and Evolution*, vol. 6, pp. 121–132, 2015.

[82] R. Cheng and T. Iles, "Confidence Bands for Cumulative Distribution Functions of Continuous Random Variables," *Technometrics*, vol. 25, no. 1, 1983.

[83] R. Cheng and T. Iles, "One-Sided Confidence Bands for Cumulative Distribution Functions," *Technometrics*, vol. 30, no. 2, 1988.

[84] R. Schobi and B. Sudret, "PCE-Based Sobol' Indices for Probability-Boxes," *8th International Conference : Sensitivity Analysis of Model Output: Celebrating the 90th Birthday of Ilya M. Sobol'*, pp. 83–84, 2016.

[85] A. Saltelli, P. Annoni, I. Azzini, F. Campolongo, M. Ratto, and S. Tarantola, "Variance Based Sensitivity Analysis of Model," *Computer Physics Communications*, vol. 181, pp. 259–270, 2010.